

Thus, it is easy to deduce that a linear (horizontal) array of dihedrons with 90° of angular aperture (with a vertical edge of flat intersection) placed on a warped surface is a very good alternative to current commercial catadioptric devices for retro-directive applications in cars. Obviously, it is also possible to make the same assertion about invisibility applications, using dihedrons of 120° if the observer movement is also restricted to the horizontal plane; even more so in this type of applications, due to the dispersive characteristics of both types of dihedrons (90° and 120°), when sight lines are placed outside the horizontal plane.

6. CONCLUSION

This document has shown that inverted cone structures of 90° and 120° of aperture can be used as retrodirective and invisible devices with a broad margin of angular aperture ($>50^\circ$).

It has also been demonstrated that an array of several inverted cones provides similar behavior, but this structure adds the advantages of a reduced thickness and the possibility to be warped without serious loss of performance. Consequently, it allows shield structures to be formed around any target independently of its size and geometry for either kind of applications (retrodirectivity and invisibility).

In the case of retrodirectivity, it has also been demonstrated that a laboratory prototype of an array structure of inverted cones with 90° of angular aperture presents better and more stable behavior than a commercial device used in vehicles as a catadioptric element.

Moreover, the novelty of this structural geometry should be highlighted, which, in the case of retrodirectivity applications, could be a good alternative to commercial devices based on similar physical concepts. The structure of inverted cones with 120° of angular aperture could provide a good alternative to current technology of shielded paints for invisibility applications, and could provide a good alternative to obtain better signal distribution within buildings as a dispersive element for Wi-Fi and Li-Fi technologies.

ACKNOWLEDGMENTS

The authors thank Julio Gutiérrez Ríos of the Faculty of Information Technology of the Polytechnic University of Madrid (UPM) for the comparative measurements carried out with its fluorescence sensor.

The work at the Complutense University of Madrid (UCM) has been partially sponsored by the Spanish Ministry of Economy and Competitiveness and by the European Regional Development Fund (ERDF) under the project MTM2014-54141-P "Algebra-geometric constructions: fundamentals, algorithms and applications".

The work at the University of Cantabria (UC) has been sponsored by the Spanish Ministry of Economy and Competitiveness through the project TEC2014-58341-C4-1-R.

The work at the Spanish Council for Scientific Research (CSIC) has been internally sponsored by the Group of Antenna Technology of the "Leonardo Torres Quevedo" Institute of Physics Technology (ITEFI).

REFERENCES

1. L.C. Van Atta, Electromagnetic reflector, US Patent 2,908,002, October 1959.
2. N. Mercé, H. Palacios, A. Pedreira, P. Tejedor, and J. Vassal'lo, Planar retrodirective reflectors, International Conference on Electromagnetics in Advanced Applications (ICEAA'99), Turin, Italy, 1999.

3. L. Cabria, J.A. García, T. Aballo, and Z. Popovic, Polar Phase-Conjugating Active Arrays for Spectrally-Efficient Linear Wireless Links, 2010 IEEE MTT-S International Microwave Symposium Digest, Anaheim, CA, 2010, pp. 77–80.
4. M. Fairouz and M. Saed, A retrodirective array with reduced surface waves for wireless power transfer applications, Progress in Electromagnetics Research C 55 (2014), 179–186.
5. M.G.J. Minnaert, Light and Colour in the Outdoors, Springer-Verlag Edit., ISBN 978-1-4612-2722-9, 1993.
6. R. Greenler, Rainbows, Halos and Glories, Cambridge University Press, ISBN 978-0521388658, January 26, 1990.
7. J. Fischer, T. Ergin, and M. Wegener, Three-dimensional polarization-independent visible-frequency carpet invisibility cloak, Optics Letters 36 (2011).
8. F. L. Metamateriales, Y. L. Xu, W. S. Fegadolli, M. H. Lu, J. E. B. Oliveira, V. R. Almeida, Y. F. Chen, and A. Scherer, Experimental demonstration of a unidirectional reflectionless parity-time metamaterial at optical frequencies, Nature Materials 12 (2013), 108–113.
9. J.A. García, R. Gonzalo, J. Gutiérrez-Ríos, A. Tazón, and J. Vassal'lo, Contribution to the improvement of flat reflectors, 2nd Meeting of the COST IC 0603, Bonn (Germany), 2007.
10. A. Pedreira and J. Vassal'lo, Anechoic Reflector, 30th European Microwave Conference (EuMC 2000), Paris, France, 2000.
11. B. Nair and V. F. Fusco, Planar printed self-channelling scatterer, Electronic Letters v39 (2003).
12. J. Gutiérrez-Ríos and J. Vassal'lo, Electromagnetic reflector without echo in the incident direction of the signal, ES 2.374.125 B1 Spanish Patent, date of priority 01/06/2009, published by the OEPM in the date 19/12/2012.
13. H. Haral, Wireless data from every light bulb, TED Global, Edinburgh, 2011.
14. Y. Wang, S. Videv, and H. Haas, Dynamic Load Balancing with Handover in Hybrid Li-Fi and Wi-Fi Networks, 2014 IEEE 25th International Symposium on Personal, Indoor and Mobile Radio Communications, 2014, pp. 574–579.
15. N. Al Abdulsalam, R. Al Hajri, Z. Al Abri, Z. Al Lawati, and M. Bait-Suwailem Mohammed, Design and Implementation of a Vehicle to Vehicle Communication System Using Li-Fi Technology, 2015 International Conference on Information and Communication Technology Research (ICTRC 2015), 2015, pp. 136–139.
16. J. Gutiérrez-Ríos, J. Vassal'lo-Sanz, J. Vassal'lo-Saco, I. Soto, E. Gallego, P. Maraver, A.E. Orobio, and A. Medrano, Sensor of fluorescent substances, U201100703 Spanish Patent, date of priority 23/05/2008, published by the OEPM (17/04/2012), BOPI-T2 page 8415, ISSN 1889-1292

© 2016 Wiley Periodicals, Inc.

METAMATERIAL-INSPIRED MICROWAVE SENSOR FOR MEASUREMENT OF COMPLEX PERMITTIVITY OF MATERIALS

Aakriti Raj,¹ Abhishek Kumar Jha,² M. Arif Hussain Ansari,¹ M. Jaleel Akhtar,^{1,2} and Sidhartha Panda¹

¹Materials Science Programme, Indian Institute of Technology Kanpur, Uttar Pradesh 208016, India

²Department of Electrical Engineering, Indian Institute of Technology Kanpur, Uttar Pradesh 208016, India; Corresponding Author: akjha.rf@gmail.com

Received 22 March 2016

ABSTRACT: This article presents the design and development of a metamaterial inspired planar microwave sensor for the measurement of complex permittivity of the solid and liquid sample under test (SUT). A hexagonal complementary split ring resonator (CSSR) is etched on the ground plane of a 50Ω microstrip line, which is excited by the electric

field component normal to the ground plane. The proposed hexagonal sensor possesses a good sensitivity, and the SUT placed over the CSSR perturbs the electric field associated with the CSRR giving rise to a change in the resonance frequency and peak attenuation of the transmission coefficient under loaded condition. An empirical relation between sensor resonance characteristics and the complex permittivity of the SUT is derived to determine the complex permittivity of the SUT. The designed sensor is fabricated on an FR4 substrate and is experimentally validated for various standard solid samples and hazardous chemical liquids. The proposed sensor is working in the frequency range of 5.3–8.2 GHz and is capable of measuring a number of samples with their dielectric properties varying over a wide range. © 2016 Wiley Periodicals, Inc. *Microwave Opt Technol Lett* 58:2577–2581, 2016; View this article online at wileyonlinelibrary.com. DOI 10.1002/mop.30106

Key words: complex permittivity; CSRR; planar sensor; metamaterial-inspired sensor

1. INTRODUCTION

Electrical characterization of materials in RF and Microwave regimes is desired in many applications covering industrial and scientific fields [1]. Every material has a unique set of electrical characteristics, and accurate measurements of these properties can provide scientists and engineers with valuable information. This information properly incorporates the materials into its intended applications for more solid designs and helps to monitor a manufacturing process for improved quality control. There are numerous techniques of permittivity measurement, and the choice of technique usually depends on material, type, frequency applications etc. Each method has its own merits and limitations. The microwave methods for materials characterization generally fall into two categories namely resonant methods and nonresonant methods. The nonresonant methods are often used to get general information about electromagnetic properties over a wide frequency range. The resonant methods, however, provide accurate knowledge of dielectric properties of low lossy materials at a single frequency or several discrete frequency points [2].

Recently, the metamaterial inspired sensors have been proposed as an alternative to the conventional cavity perturbation technique, which is well suited for sensing applications [3]. Lately, many metamaterial-based sensors with the single splitting resonator (SRR) coupled microstrip line for material characterization have been presented [4,5]. However, the sensitivity of the device based on SRR has not been enough to discriminate small changes in the permittivity of the sample. In order to alleviate this problem, a rectangular complementary split-ring resonator (CSRR) has been proposed for complex permittivity extraction of liquid samples. The CSRR provides a larger area of fringing electric field as compared to the SRR that increases the effective interaction area with the sample and hence increases the sensitivity of the device [6].

In this paper, the hexagonal CSRR based metamaterial inspired planar sensor is proposed for the complex permittivity characterization of the sample under test (SUT). The proposed hexagonal CSRR is compared with the rectangular CSRR given in [5], and it is observed that the hexagonal CSRR based sensor has better sensitivity as compared with the rectangular one. The proposed sensor resonating at 8.2 GHz is designed and modeled using the full wave electromagnetic solver, the CST microwave Studio. The introduction of the SUT over the CSSR perturbs the resonant frequency and the peak attenuation in transmission characteristic of the unloaded sensor. The impact of the real (ϵ'_r) and imaginary (ϵ''_r) parts of complex permittivity of SUT on resonant frequency and peak attenuation is observed, and the

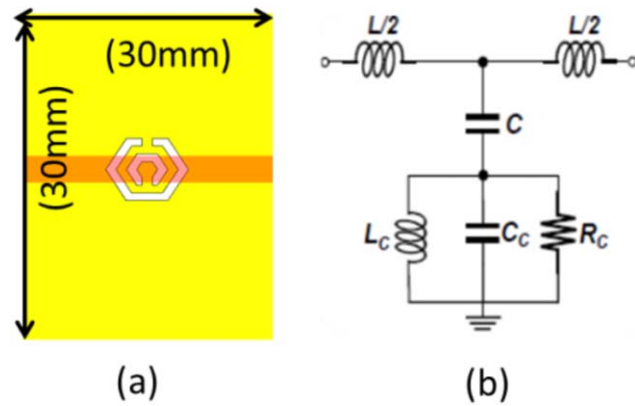


Figure 1 (a) CSRR coupled microstrip line. (b) The equivalent lumped circuit model for single CSRR coupled with microstrip line. [Color figure can be viewed in the online issue, which is available at wileyonlinelibrary.com.]

obtained numerical data are used to derive empirical relations for the calculation of complex permittivity. The proposed sensor is realized on a 0.8 mm FR4 substrate using the standard photolithography technique and is ultimately used for characterization of various solid and hazardous chemical liquid samples. The accuracy of the fabricated sensor is verified with data available in the literature for both solid and liquid samples. For the hazardous liquid samples, the data obtained from the standard probe method is used as the reference, while for solid samples the reference values are taken from literature [7]. A good agreement is observed between the measured complex permittivity values and the reference data.

2. PRINCIPLE

The working principle of the designed sensor is based on the electric field perturbation theory. The resonant frequency and quality factor of the designed sensor changes due to change in effective capacitance of the designed CSRR due to perturbation in electric field intensity associated with the CSRR. The metamaterial inspired sensor and its equivalent electrical lumped circuit model [8] are shown in Figure 1. The term L represents the line inductance of the microstrip line, C is termed as the coupling capacitance between the microstrip line and the etched CSRR in the ground plane, L_c is the inductance induced across the etched CSRR, C_c is developed capacitance inside the etched CSRR, and R_c represents the resistive part associated with the CSRR. The resonant frequency and the quality factor of the CSRR based sensor can be given as (1) and (2), respectively [5].

$$f_r = \frac{1}{2\pi\sqrt{L_c + (C_c + C)}} \quad (1)$$

$$Q = \frac{R\sqrt{(C_c + C)}}{\sqrt{L_c}} \quad (2)$$

when a dielectric material under test is placed over the CSRR, the term L_c will be constant because the length of the circular loop is fixed for designed CSRR, and C is also assumed to be constant because of the FR4 substrate having fixed dielectric constant. The capacitance of the CSRR, C_c will change moderately with the change in the effective dielectric constant value of SUT. The C_c in term of dielectric constant of SUT is approximately given as

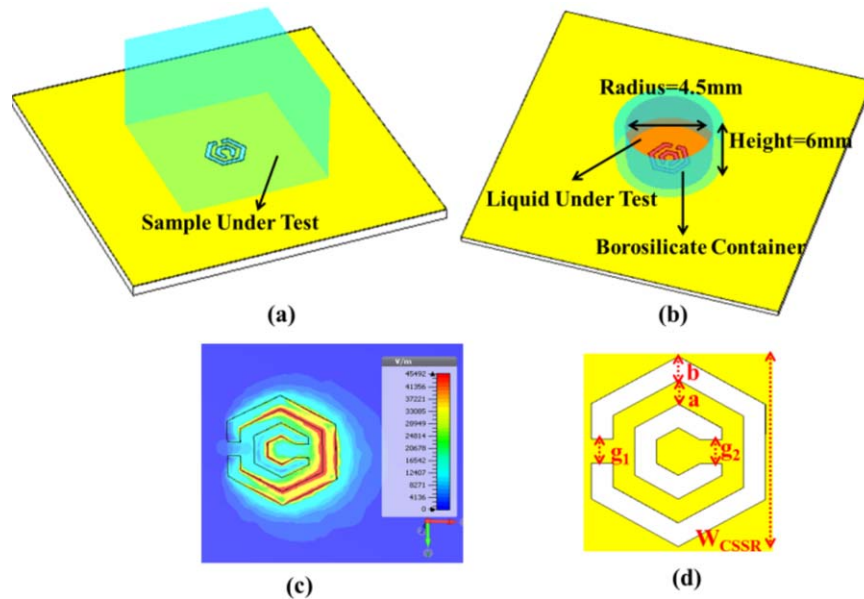


Figure 2 Simulated model (a) Perspective view of sensor Loaded with sample, (b) bottom view of sensor etched with CSRR, (c) electric Field Distribution of sensor at 8.28 GHz, and (d) geometry of CSRR. [Color figure can be viewed in the online issue, which is available at wileyonlinelibrary.com.]

$$C_c = C_0 + \epsilon'_r C_{MUT} \quad (3)$$

where C_0 is the capacitance of the CSRR without SUT, and $\epsilon'_r C_{MUT}$ is the effective capacitance in the presence of SUT. The symbol ϵ'_r is the real part of the complex permittivity ϵ_r of the SUT, which is given by

$$\epsilon_r = \epsilon'_r - j''_r \quad (4)$$

From (1)–(3), it can be concluded that the resonance frequency and the quality factor of the sensor are the functions of the complex permittivity of the SUT. The changes in resonant frequency and the quality factor can be mapped to the complex permittivity of the SUT using an empirical relation, which is derived in next section.

3. DESIGN AND NUMERICAL SIMULATIONS FOR SOLID AND HAZARDOUS LIQUID SAMPLES

The proposed sensor model for the solid characterization is shown in Figure 2(a), which is designed to resonate at 8.2 GHz. The same model can also be used for the characterization of liquid samples by utilizing a sample holder made of borosilicate container having a larger cross-sectional area as compared to the

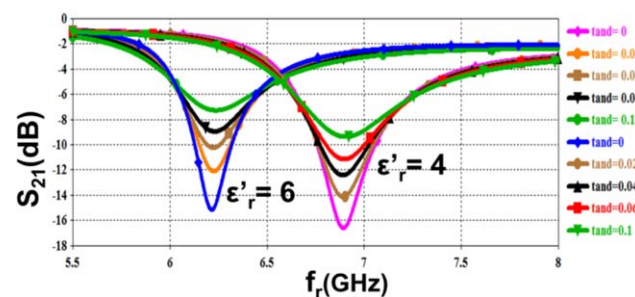


Figure 3 Transmission coefficient of the proposed hexagonal sensor simulated using CST. [Color figure can be viewed in the online issue, which is available at wileyonlinelibrary.com.]

designed CSRR unit as shown in Figure 2(b). The electric field distribution of the hexagonal CSRR based sensor is given in Figure 2(c). The hexagonal CSRR with the optimized dimensions ($g_1 = 0.43$ mm, $a = 0.40$ mm, $g_2 = 0.43$ mm, $b = 0.58$ mm, and $W_{CSSR} = 4$ mm) is shown in Figure 2(d).

It can be seen from Figure 2(c) that the maximum electric field concentration occurs near the capacitive open loop making this area highly sensitive for dielectric characterization as shown in Figure 2(c). Therefore, the solid sample is placed directly over the hexagonal CSRR where the electric field perturbation would be maximum. The response of the designed sensor corresponding to the variation in complex permittivity of SUT viz. $\epsilon'_r = 4$ to 6 and $\tan \delta = 0$ to 0.1 in terms of numerically calculated transmission coefficients is shown in Figure 3.

It is observed from Figure 3 that the change in resonant frequency is more significant with the variation in ϵ'_r in comparison to $\tan \delta$ variation, whereas $\tan \delta$ has a higher impact on the peak attenuation of S_{21} (dB) as compared with ϵ'_r . In this article, for

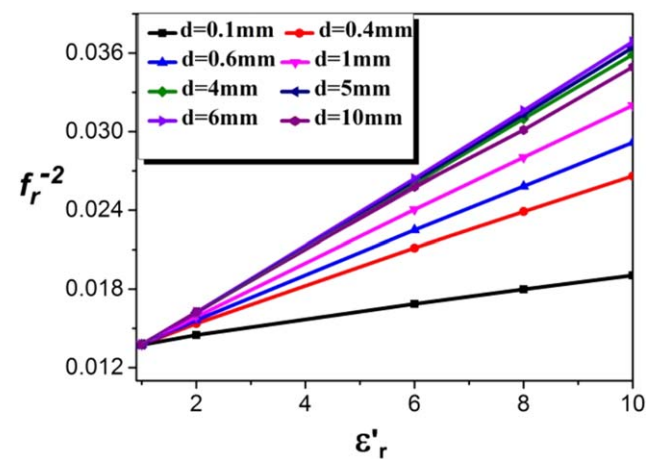


Figure 4 Effect of sample thickness variation on the resonant frequency of the proposed metamaterial-inspired sensor. [Color figure can be viewed in the online issue, which is available at wileyonlinelibrary.com.]

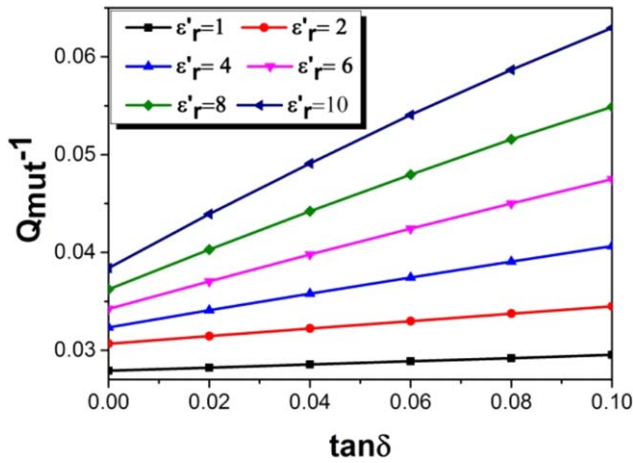


Figure 5 Plot of Q_{mut}^{-1} versus $\tan \delta$ at frequency 8.28 GHz. [Color figure can be viewed in the online issue, which is available at wileyonlinelibrary.com.]

the simplicity of approach, it has been assumed that the shift in resonant frequency is due to change in ϵ'_r only while the peak attenuation of S_{21} (dB) is mainly affected by $\tan \delta$ variation.

3.1. Numerical Model for the Real Permittivity

To derive a numerical model for the real permittivity, the resonant frequencies corresponding to $\epsilon'_r=1$ to 10 and sample thickness $d=0.1$ to 10 mm have been recorded. The inverse square of resonant frequency f_r^{-2} with ϵ'_r for different sample thickness is plotted in Figure 4. It is observed from Figure 4 that the variation of f_r^{-2} with ϵ'_r is linear whereas slope of the straight line is changing with a variation of the thickness of the material under test. It is interesting to note that the slope variation is almost constant for the sample thickness >5 mm. In this article, for simplicity of the approach, the effect of sample thickness is nullified by taking the all the measured sample >5 mm thick and, therefore, the height of the liquid container for SUT is also taken as 6 mm. The plotted data in Figure 4 is fitted using commercially available software Origin Pro 9.1 to obtain the equation for ϵ'_r calculation in terms of resonant frequency for both solid and liquid characterization and given as

$$\epsilon'_r = \frac{f_r^{-2} - 0.0119933}{0.0023433} \quad (5)$$

3.2. Numerical Model for Loss Tangent

To derive the numerical model for loss tangent calculation, the peak attenuation of each curve corresponding to $\epsilon'_r=1$ to 10 and

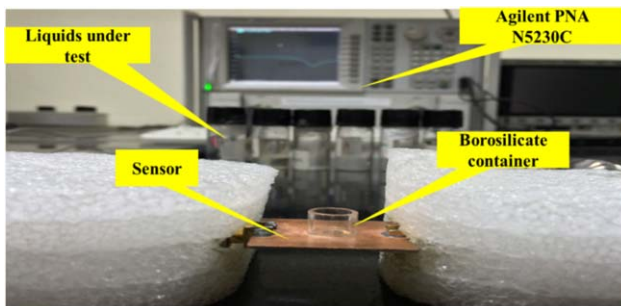


Figure 6 Measurement setup of the fabricated device equipped with borosilicate sample container. [Color figure can be viewed in the online issue, which is available at wileyonlinelibrary.com.]

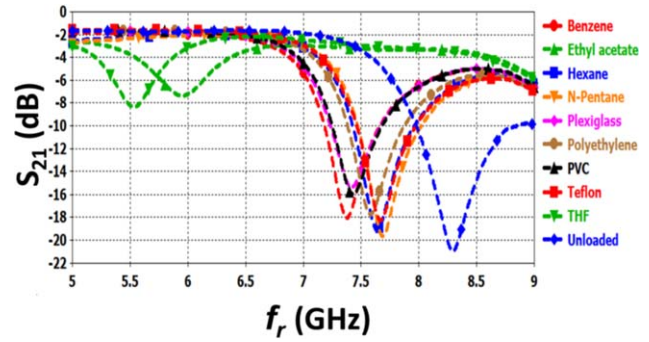


Figure 7 Measured S_{21} (dB) corresponding to various standard solid and liquid samples. [Color figure can be viewed in the online issue, which is available at wileyonlinelibrary.com.]

$\tan \delta=0$ to 0.1 is recorded in case of liquid samples whereas $\epsilon'_r=1$ to 10 and $\tan \delta=0$ to 0.01 is considered in case of the solid samples. The quality factor corresponding to each S_{21} (dB) magnitude is calculated from (6) [7].

$$Q_{mut} = Q_U \left(1 - 10^{\frac{S_{21}(\text{dB})}{20}} \right) \quad (6)$$

The inverse of quality factor Q_{mut}^{-1} with $\tan \delta$ of the SUT is plotted in Figure 5. It is noted from Figure 5 that the plotted curve is a straight line with slope dependent on ϵ'_r . The equation for $\tan \delta$ in terms of Q_{mut}^{-1} and ϵ'_r is derived from the curve plotted in Figure 5, which is given in (7) for liquid samples.

$$\tan \delta = \frac{Q_{mut}^{-1} + 0.0036(\epsilon_r'^2) - 0.0324(\epsilon_r') - 0.0182}{0.0358(\epsilon_r'^2) - 0.2514(\epsilon_r') + 0.3517} \quad (7)$$

4. MEASUREMENTS AND RESULTS

The proposed hexagonal sensor is fabricated on an FR4 substrate using the microstrip technology and the complete measurement setup for liquid SUT testing using the vector network analyzer (VNA) is shown in Figure 6. The quality factor and the resonant frequency are obtained from the measured transmission coefficients. The sensor is connected with VNA through coaxial

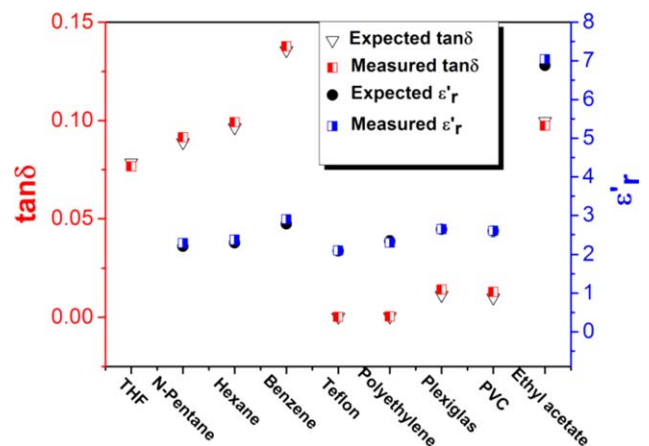


Figure 8 Comparison of results measured using the proposed metamaterial-inspired sensor with the reference values of various standard samples under test. [Color figure can be viewed in the online issue, which is available at wileyonlinelibrary.com.]

SMA connectors. Prior to the measurement, a short-open-load-through (SOLT) calibration is performed using the Agilent probe kit 85052D. The intermediate frequency bandwidth is set to 100 Hz, and the number of sweeping points is taken as 1601 for better clarity. Various standard samples, namely, Teflon, PVC, Plexiglas, and Polyethylene, in the case of solids, and tetrahydrofuran, benzene, hexane, ethyl acetate, and *n*-pentane in the case of hazardous liquid samples are measured to record the corresponding resonant frequency (f_r) and the quality factor. These measured data are then used in the derived numerical model (5) and (7) to get the dielectric constant and loss tangent of SUT, respectively. The measured results are shown in Figure 7.

The calculated dielectric constant and loss tangent values from the measured set of resonant frequency (f_r) and the quality factor data are shown graphically in Figure 8. The calculated data are then compared with the published data [6] in the case of solid samples and with the data obtained from the conventional coaxial probe in the case of hazardous liquid samples. The comparison of these measured and reference data are shown in Figure 8. From this figure, it is observed that a good match is found between the reference data and the measured values obtained using the proposed method, which involves the metamaterial based hexagonal CSRR as a sensing element.

5. CONCLUSION

In this article, a metamaterial inspired hexagonal CSRR based microstrip sensor has been presented for microwave characterization of dielectric materials. The numerical model has been developed for estimating the complex permittivity of the SUT in terms of the resonant frequency and the transmission coefficient. The measurement has been performed for various standard solid as well as liquid samples, and it has been found that the measured results are in close agreement with the published data and with the dielectric probe kit data at the operating frequency. The designed sensor provides a viable approach possessing a good sensitivity for complex permittivity extraction of various solid and liquid samples in RF and microwave frequency band.

REFERENCES

1. A. R. V. Hippel, Dielectric materials and applications, Wiley, New York, 1954.
2. James Baker-Jarvis, R. G. Geyer, J. H. Grosvenor, M. D. Janezic, C. A. Jones, B. Riddle, C. M. Weil, and J. Krupka, Dielectric characterization of low-loss materials a comparison of techniques, *IEEE Trans Dielectr Electr Insul* 5 (1998), 571–577.
3. M. Arif Hussain, Abhishek Kumar Jha, and M. J. Akhtar, Design of CSRR based planar sensor for non-invasive measurement of complex permittivity, *IEEE Sens J* 15 (2015), 7181–7189.
4. L. Hee-Jo, L. Jung-Hyun, M. Hui-Sung, J. Ik-Soon, C. Jong-Soon, Y. Jong-Gwan, and J. Hyo-II, A planar split-ring resonator-based microwave biosensor for label-free detection of biomolecules, *Sens Actuators Chem* 169 (2012), 26–31.
5. W. Withayachumnankul, K. Jaruwongrungrsee, A. Tuantranont, C. Fumeaux, and D. Abbott, Metamaterial-based microfluidic sensor for dielectric characterization, *Sens Actuators A: Phys* 189 (2013), 233–237.
6. A. Ebrahimi, W. Withayachumnankul, S. Al-Sarawi, and D. Abbott, High-sensitivity metamaterial-inspired sensor for microfluidic dielectric characterization, *IEEE Sens J* 14 (2014), 1345–1351.
7. A. K. Jha and M. J. Akhtar, A generalized rectangular cavity approach for determination of complex permittivity of materials, *IEEE Trans Instrum Meas* 63 (2014), 2632–2641.
8. K. Chang and H. Lung-Hwa, Microwave ring circuits and related structures, 2nd ed., Wiley, Hoboken, NJ, 2004.

A COMPARATIVE STUDY OF DIFFERENT GAIN CELLS BASED MICROWAVE CMOS DISTRIBUTED OSCILLATORS

Kalyan Bhattacharyya¹ and D. K. Sharma²

¹Department of Electronics and Communications Engineering, Amrita School of Engineering, Amrita Vishwa Vidyapeetham University, Amrita University, Coimbatore, India

²Department of Electrical Engineering, Indian Institute of Technology Bombay, Mumbai 400076, India; Corresponding author: b_kalyan@cb.amrita.edu

Received 23 March 2016

ABSTRACT: Different gain cells used for Distributed oscillators (DOs) have been studied through extensive simulations. Measured results for a cascode DO are also reported, with oscillation frequency of around 10.1 GHz with 4.63 dBm output power at 1.8 V and phase noise of -114 dBc/Hz at 1 MHz offset from the carrier. © 2016 Wiley Periodicals, Inc. *Microwave Opt Technol Lett* 58:2581–2587, 2016; View this article online at wileyonlinelibrary.com. DOI 10.1002/mop.30105

Key words: distributed oscillator; voltage controlled oscillator; coplanar waveguide; body bias; phase noise

1. INTRODUCTION

High frequency performance of devices is often restricted by the electrode capacitance associated with them. One way of getting around this limitation is to make these capacitances a part of tuned circuits or to absorb these into transmission line parameters. Distributed amplifiers (DAs) make use of the latter technique. The amplifying element (called the gain cell) is split into multiple parts connected by transmission lines. This technique has been known for a long time. The term DA was introduced by Ginzton, Hewlet, Jasberg, and Noe in 1948 [1] for amplifiers implemented with vacuum tubes. Lately, scaled down CMOS technologies have acquired the ability to work at microwave frequencies. This is an attractive option because CMOS is a low-cost, low-power technology.

Different gain cells have been suggested in literature for DAs and Oscillators (DOs) [2–9] in different processes. However, there is no proper comparison between DOs using these different gain cells. A fair comparison requires that all DOs be implemented in the same process. Proper post layout simulations should be used to compare characteristics of gain cells as well as the performance parameters of Distributed Oscillators using these. A number of gain cells have been suggested in literature [7–9] to achieve different desirable characteristics of DAs or distributed oscillators (DOs). Commonly used gain cell are n-MOSFET [2,4], and n-MOSFETs cascode [5,6,10]. We have also proposed n–p MOSFET gain cell earlier in Ref. 8 i.e. n-MOSFET common source (CS) with p-MOSFET passive load. Xin Guan and Cam Nguyen [7] also suggested the possibility of using CMOS inverters as gain cells and we have also used this in Ref. 9.

Figure 1 shows the three gain cells other than a simple CS NMOSFET. Figure 1(a) shows the cascode cell, Figure 1(b) shows a CS NMOSFET with a PMOS load and Figure 1(c) shows the CMOS inverter used as a gain cell.

2. DESIGN OF GAIN CELLS

Performance of DAs and DOs is decided largely by the gain cells they use. It is of interest to study the suitability of these gain cells for different types of applications. While data are available for these in published literature, it is difficult to do a